CO₂ Wetting on Pillar-Nanostructured Substrates

Jianyang Wu,[1,2,*] Ingrid Snustad,[1,3] Åsmund Ervik,[3] Amy Brunsvold,[3] Jianying He[1] and Zhiliang Zhang[1,*]

[1]NTNU Nanomechanical Lab, Norwegian University of Science and Technology (NTNU), Trondheim 7491, Norway

[2]Department of Physics, Research Institute for Biomimetics and Soft Matter, Jiujiang Research Institute and Fujian Provincial Key Laboratory for Soft Functional Materials Research, Xiamen University, Xiamen 361005, P.R. China

[3]SINTEF Energy Research, P.O. Box 4761 Sluppen, 7465 Trondheim, Norway

Abstract: CO₂ capture by dropwise CO₂ condensation on cold solid surfaces is a promising technology. Understanding the role of nanoscale surface and topographical features on the CO₂ droplet wetting characteristics is of importance for CO₂ capture by this technology, but this remains unexplored yet. Here, using large-scale molecular dynamics (MD) simulations, the contact angle and wetting behaviors of CO₂ droplets on pillar-structured Cu-like surfaces are for the first time investigated. Dynamic wetting simulations show that, by changing the strength of the solid-liquid attraction $\varepsilon_{\text{Cu}-\text{CO}_2}$, smooth Cu-like surface offers a transition from CO₂-philic to CO₂-phobic. By periodically pillared roughening of the Cu-like surfaces, however, a higher contact angle and a smaller spreading exponent of liquid CO₂ droplet are realized. Particularly, a critical crossover of CO₂-philic to CO₂-phobic can appear. The wetting of pillared surfaces by liquid CO₂ droplet is non-uniformly proceeded. The liquid CO₂ droplet is capable of exhibiting a transition from the Cassie state to the Wenzel state with increasing $\varepsilon_{\text{Cu}-\text{CO}_2}$, increasing inter-pillar distance and increasing pillar width. The wetting morphologies of metastable Wenzel state of the CO₂ droplet are very different from each other. The findings will inform the ongoing design of CO₂-phobic solid surfaces for practical dropwise condensation-based CO₂ capture applications.

---

*Corresponding Emails: jianyang@xmu.edu.cn, zhiliang.zhang@ntnu.no

Keywords: Pillar-structured surfaces; CO_2 droplet; Contact angle; Molecular dynamics

1. Introduction

Carbon dioxide (CO_2) is one of the predominant greenhouse gases in strengthening the global climate change. Remarkable reduction in anthropogenic release of CO_2 gas is urgently required to mitigate and reverse the global warming process for environmental protection and sustainable development. On the other hand, CO_2 is also an important substance for versatile practical applications, for example, as a carbon source for producing many chemicals[1-3]. Carbon capture and storage (CCS) from large-scale emission sources not only brings economic benefits but also mitigates global climate change concerns[4-5]. As a key step in the CCS process, the CO_2 capture dominates the total cost[6]. Therefore, developing a practical and economically viable approach for CO_2 capture is currently not only a scientific research interest but also a social issue for environmental protection.

In the past few decades, there have been a number of techniques proposed for CO_2 capture, including physical/chemical absorption, adsorption, membrane, gas hydrate, etc[4-7]. However, each standalone technology is facing several challenges. For instance, the drawbacks of absorption-based technique include high corrosion rate of equipment, degradation of solvent, negative environmental impact of solvent emission, etc[6, 8-10]. Adsorption-based CO_2 capture process shows disadvantages of relatively low CO_2 selectivity, low adsorption rate, sorbent degradation, attrition in cyclic operation, intermittent operation, and so on[6, 11-13]. Membrane-based approach is plagued with requirement of compression for driving force, requirement of high selectivity, fouling effect, high surface area of membrane, moisture induced low permeability of polymer membrane, etc[14-17]. Hydrate-based CO_2 capture shows low efficiency due to other molecules trapped in the clathrate cage structures and secondary pollution of clathrate hydrate promoter[18-20]. As a result, there is thus still a request to develop alternative cost-effective methods for large-scale CO_2 capture.

Very recently, inspired by that bulk water is collected from fog or humid air atmosphere through water droplet condensation on solid surfaces with hydrophobicity [21-22] or hierarchical nanostructures[23-24], a promising technology of CO_2 capture based on dropwise CO_2 condensation on cooled structures

was accordingly suggested[25-26]. Similar to the case of water, it is expected that liquid CO_2 droplets nucleate onto cold CO_2-phobic surfaces in a CO_2 vapor environment. Under the action of gravity and gas streams, nucleated/condensed droplets can be readily collected from the surfaces, enabling a potentially improved low-temperature capture technique. A key advantage of the low-temperature process is that the captured CO_2 is produced directly in the liquid state and does not need energy-intensive processing before it can be transported away. The benefit of CO_2 capture by this technology is controlled by the CO_2-phobicity of contacting surfaces. Particularly, the wettability, evaporation and condensation of CO_2/solid wall systems play a key role in this novel technology. Because CO_2 is often utilized in petroleum engineering, for example, CO_2-enhanced gas and oil recovery (CO_2-EGR and CO_2-EOR) in depleting petroleum fields[27-30], a large number of experimental and theoretical investigations have focused on the wetting properties in confined structures under different environments[31-40]. As an example, using molecular simulations, the microstructures, dynamics, and recovery rate of CO_2-EOR in nanochannels were investigated[39]. Using large-scale molecular dynamics (MD) simulations, in the presence of a bulk aqueous phase, supercritical CO_2 forms a non-wetting droplet above the hydrophilic kaolinite surface, whereas in the presence of bulk supercritical CO_2, non-wetting aqueous droplets interact with the hydrophobic kaolinite surface via a mixture of adsorbed CO_2 and H_2O molecules[33]. It is also revealed that the presence of CO_2 gas alters the wetting behaviors of water droplet on solid surfaces[36, 38, 41-42].

To date, however, fundamental research on the wetting, evaporation and condensation behaviors on solid substances in CO_2 atmosphere without confinement are largely limited, but this is of crucial for dropwise condensation-based CO_2 capture. As is well-known, by engineering micro-/nano-textured surfaces, hydrophobic surfaces can become more hydrophobic, or even super-hydrophobic[43-46]. A question immediately arises as to whether textured structures will alter or enhance their CO_2-phobicity similar to hydrophobic surfaces? In the present work, the contact angle and wetting behaviors of a CO_2

droplet on Cu-like solid substrate with pillar-structured surfaces are for the first time characterized by means of large-scale MD simulations.

2. Models and Method

Because copper (Cu) material shows excellent heat transport properties, a Cu substance is considered into investigation in this study. To examine the effects of surface roughness on the wetting characteristics of CO_2 droplets, five distinct nanotextured surfaces that are structurally characterized by a square pillar array with constant height $H = 100.0$ Å, varying width w and inter-pillar spacing w in the range of around 10.7 - 71.4 Å, are generated. In addition, a flat surface is also created as a reference. Figure 1a and b shows the molecular models containing a smooth surface and a pillared surface with $w = 71.4$ Å, respectively. All investigated substrates are composed of Cu atoms with face-centered-cubic (*fcc*) latticed arrangement and show identical horizontal xy dimensions of 428.6×428.6 Å^2. The top surfaces of all substrates are the (100) surface that shows low surface energy. A cuboid CO_2 droplet with *fcc* latticed arrangement is initially placed over the surface with a gap of 10 Å. The droplet relaxes into a spherical liquid shape in the initial part of the simulation before touching the solid surface. Figure 1c presents an atomic model of partial pillar-structured surface with $H = 100.0$Å and $w = 71.4$ Å.

To describe the interactions of atoms in the systems, a hybrid forcefield is employed. For the *fcc* Cu substrate, a many-body forcefield of the embedded-atom-method (EAM) is utilized to mimic the atomic interactions[47]. Based on this EAM potential, the total potential energy of a metallic system is expressed as[48]

$$E = \frac{1}{2}\sum_{ij} U\left(r_{ij}\right) + \sum_{ij} U\left(\bar{\rho}_i\right)$$

(1)

where $U\left(r_{ij}\right)$ and $U\left(\bar{\rho}_i\right)$ are a pairwise potential with respective to the atomic distance of atom i and j, and the embedding energy for placing an atom i into the host electron density that is calculated from

other atoms in the system. This EAM forcefield reproduces the structural and mechanical properties of perfect and defects-contained Cu materials[47].

With regard to the case of CO_2, a coarse-grained (CG) forcefield named as SAFT-γ *Mie* potential[49] is employed to describe the intermolecular interactions of the CO_2 system. The function of the SAFT-γ *Mie* potential is mathematically written as[49]

$$E^{Mie}(d) = \varepsilon C(\lambda_r, \lambda_a) \left[\left(\frac{\sigma}{d} \right)^{\lambda_r} - \left(\frac{\sigma}{d} \right)^{\lambda_a} \right]$$

(2)

with

$$C(\lambda_r, \lambda_a) = \left(\frac{\lambda_r}{\lambda_r - \lambda_a} \right) \left(\frac{\lambda_r}{\lambda_a} \right)^{\left(\frac{\lambda_a}{\lambda_r - \lambda_a} \right)}$$

(3)

where d, ε and σ are the distance between CG CO_2 molecules, the well depth of the *Mie* potential and the diameter of the CG CO_2 molecules, respectively. In this study, the parameters σ, λ_a and λ_r in the *Mie* potential of CG CO_2 particles are taken as 3.741, 6.66 and 23.0, respectively[49]. It was showed that the SAFT-γ *Mie* potential with those parameters can efficiently and accurately predict the structural and dynamics properties of vapor, liquid and vapor-liquid CO_2 systems[26, 50-51].

As for the unlike-pair atomic interactions between substrates and CO_2, the *Mie* potential is also used. To well investigate the wetting morphology of CO_2 droplet, the critical energy interaction parameter is simply changed from 0.005 - 0.015 eV for fully covering the wetting properties of Cu-like surface from CO_2-phobic to CO_2-philic. A cutoff of 15.0 Å is assigned for the interactions of the *Mie* potential, which is over 4-folds of both σ for the CO_2 *Mie* and for the unlike interactions.

For the CO_2/Cu systems as shown in Figure 1a and b, periodic boundary conditions (PBCs) are adopted in the horizontal 2D *xy* dimensions, while the vertical *z* direction is non-PBC to avoid the interatomic interactions between top CO_2 molecules and bottom layers of substrate. To maintain a

constant volume, a virtual wall is placed at the top with vertical position of 300.0 Å. To prevent CO_2 molecules fleeing to the vacuum space, this virtual wall is able to exert repulsive force onto each CO_2 molecule with the magnitude defined by

$$F(r) = \begin{cases} -k(r-R)^2, & r \geq R \\ 0, & r \leq R \end{cases}$$

(4)

where k is an effectively spring force constant, and r is the distance from CO_2 particle to the virtual wall. R is the cutoff at which the wall-particle interaction energy is zero. In this study, the spring constant k and the cutoff R are taken as 0.1 kcal/(mole·$Å^2$) and 5.0 Å, respectively. It is noted that the setup of those values of parameters in our MD simulations effectively prevent the escape of CO_2 molecules and does not affect the morphologies of liquid CO_2 droplet by the virtual wall.

MD simulations are performed at 223.15 K under canonical NVT (constant number of atoms, constant volume and constant temperature) ensemble, where the temperature is controlled by Nosé-Hoover thermostat. Even though NVT is used, note that since the system is in vapor-liquid equilibrium, the liquid droplet will exchange molecules with the gas until the pressure in the system corresponds to the vapor pressure at 223.15 K. The equation of atomic motions with a timestep of 5 fs is integrated by the velocity-Verlet method. Within the MD simulations, atoms in the substrate are fixed without integration of motion. A MD simulation time of 50 ns is used for equilibrating the system dynamics of the CO_2 droplet. All the MD calculations are carried out by using the large-scale atomic-molecular massively parallel simulator (LAMMPS) code package.

3. Results and Discussion

Initially, the wetting behaviors of a CO_2 droplet containing 144000 CO_2 molecules on smooth surface of Cu are studied. Figure 2a shows the side-viewed configurations of a CO_2 droplet interacting with the flat Cu-surface with varying energy interaction parameter ε_{Cu-CO_2} from 0.005-0.012 eV after simulation time of 50 ns. Clearly, a vapor-liquid-solid mixed system is achieved for each case. The

wetting morphology of the CO_2 droplet is markedly connected to ε_{Cu-CO_2}. As ε_{Cu-CO_2} changes from

0.005-0.012 eV, the surfaces of liquid CO_2 droplets are spherical, whereas for $\varepsilon_{Cu-CO_2} = 0.012$ eV, a

liquid film forms, separating the CO_2 vapor phase and the Cu substrate. It is noted that there is strong

exchange of CO_2 molecules between vapor and liquid CO_2 phase in all systems, corresponding to the

equilibrium dynamics of CO_2 evaporation and condensation. Figure 2b plots the development of

potential energy of CO_2 (E_{CO_2}) in the systems as a function of MD simulation time. It is found that

E_{CO_2} oscillates at constant values after very short time of MD relaxation, indicative of equilibrium

dynamics of the vapor-liquid CO_2 systems. Interestingly, as ε_{Cu-CO_2} varies from 0.005-0.009 eV, the

systems show almost similar total E_{CO_2} but different droplet geometries at equilibrium state. This is

mainly explained by the fact that the total E_{CO_2} is contributed by the vapor and liquid phases of CO_2

in those systems. As ε_{Cu-CO_2} becomes larger, however, E_{CO_2} is smaller because of stronger interacting

with solid surface of CO_2. Figure 2c presents the center-of-mass z positions (COMPs) of CO_2 as a

function of MD simulation time. Similarly, as the systems reach to equilibrium state within short time,

the CO_2 COMPs fluctuate at constant values. The fluctuation of COMPs is stronger as ε_{Cu-CO_2} is

smaller. The different CO_2 COMPs indicate different wetting morphologies of liquid CO_2 droplet as

shown in Figure 2a. To quantitatively differentiate the adsorbed layers of CO_2 molecules on the solid

surfaces with different ε_{Cu-CO_2}, the density distribution profiles of CO_2 are plotted in Figure 3.

Apparently, different ε_{Cu-CO_2} result in different density distribution profiles, suggesting different

structures of adsorbed layers. The number of obvious peaks reduces as ε_{Cu-CO_2} is decreased. For

example, when $\varepsilon_{Cu-CO_2} = 0.005$ eV, only one peak can be observed, however, as $\varepsilon_{Cu-CO_2} = 0.012$ eV,

five peaks can be identified. The peaks are indicative of the adsorbed CO_2 layers and higher value of

ε_{Cu-CO_2} results in higher planar density of the adsorbed layers. Interestingly, the location of peaks is

also connected with ε_{Cu-CO_2}. As ε_{Cu-CO_2} increases from 0.005 - 0.012 eV, the location of the first peak monotonically declines from around 3.22 - 2.96 Å, indicating different gaps between surface and the first CO_2 layer. For all cases, however, the neighboring distances between peaks are around 3.50 Å, which is insensitive to ε_{Cu-CO_2}.

Figure 4a compares the side-viewed wetting morphologies of a CO_2 droplet on a pillar-structured Cu surface with different ε_{Cu-CO_2} after MD simulation time of total 50 ns. Similar to the smooth surface, a vapor-liquid-solid system is realized and the contact area between CO_2 droplet and top surface varies with ε_{Cu-CO_2}. However, there are clear differences between the wetting morphologies of droplet on smooth and pillared surfaces with identical ε_{Cu-CO_2}. As ε_{Cu-CO_2} changes from 0.005 - 0.009 eV, the liquid CO_2 droplet shows partially spherical shapes above the pillared surface, preferring Wenzel state. In the Wenzel state, the space between pillars is filled with CO_2 gas. As ε_{Cu-CO_2} reaches to 0.010 eV; however, liquid CO_2 droplet is able to partially permeate into the groove, demonstrating a Cassie state. The part of liquid droplet above the pillared surface still shows partially spherical geometry. Finally, when ε_{Cu-CO_2} is over 0.010 eV, the liquid CO_2 droplet fully permeates into the groove, illustrating that the pillared surface is fully wet by the CO_2 droplet. It is also noted that strong exchange of CO_2 molecules between vapor and liquid CO_2 occurs in those systems, similar to the case of smooth surface systems. Figure 4b plots the evolution of total E_{CO_2} of the CO_2/pillared surface systems during the MD simulation under NVT ensemble. Initially, the changes in E_{CO_2} are pronounced, mainly originating from evaporation and geometry change of CO_2 liquid droplet. When ε_{Cu-CO_2} varies from 0.005 - 0.009 eV, E_{CO_2} rapidly reaches to a constant value, indicating that the system reaches to stable state. It is also found that the equilibrium E_{CO_2} increases with increasing E_{CO_2}. For ε_{Cu-CO_2} = 0.015 eV, marked reduction in the E_{CO_2} initially occurs, and then reaches to a constant value. As ε_{Cu-CO_2} = 0.012 eV,

however, E_{CO_2} initially increases, then declines, and finally reaches to a constant value. Particularly, as $\varepsilon_{Cu-CO_2} = 0.010$ eV, E_{CO_2} monotonically increases within the whole simulation time. This suggests that the system does not reach its equilibrium state. The Cassie state as shown in Figure 4a is an intermediate metastable state. Figure 4c plots the z-directional COMPs of CO_2 against MD simulation time as ε_{Cu-CO_2} increases from 0.005 - 0.015 eV. Except $\varepsilon_{Cu-CO_2} = 0.010$ eV, the z-directional COMPs are unchanged when the MD simulation time is over 20 ns. This clearly reveals that the CO_2 molecular systems reach the equilibrium state at 50 ns. Similar to the cases of CO_2/smooth surface systems, smaller ε_{Cu-CO_2} causes larger amplitude in the fluctuation of z-directional COMPs. Interestingly, when $\varepsilon_{Cu-CO_2} = 0.010$ eV, the z-directional COMP declines during the entire MD simulation time. The wetting is slowed in this case by the motion of the contact line, so it is very hard to reach true equilibrium in the Wenzel state.

The contact angle is commonly utilized to quantitatively characterize the wettability of a solid surface by a liquid droplet.[52] To extract the contact angle of a liquid CO_2 droplet on Cu-like surface, the 2D density map is accordingly obtained as follows. Initially, the COMP of the vapor plus liquid CO_2 phases is calculated. The 2D COMPs (x, y) are considered as the COMPs of the liquid CO_2 droplet system (ρ, z). The surrounding local CO_2 density is then achieved by counting the number N of CO_2 molecules in a finite circular shell with radius, width and height of r, Δr and Δz, $i.e$, $\rho = N/(2\pi r \Delta r \Delta z)$ where $\Delta r = \Delta z = 1$ Å are chosen. To diminish the fluctuation effect of local densities, the global CO_2 relative density map is finally realized by averaging densities from 50 samples in cylindrical coordinates. Figure 5a and b shows two examples of representative density contours of CO_2 on a smooth and a pillar-structured surfaces with $\varepsilon_{Cu-CO_2} = 0.008$ eV, respectively. Clearly, the density contour in Figure 5a shows evidence of red-and-white lines adjacent to the smooth Cu surface, indicating multi-layered CO_2 structures adsorbed on the surface that can also be quantified by the density profiles as shown in Figure 3. In contrast, the local CO_2 densities adjacent to the pillar-

structured surface are less enhanced as a result of less contact area between liquid droplet and solid surface. The number of CO_2 layers close to the pillar-structured surface is less than that near the smooth one. However, slightly below the top pillar-structured surface ($z < 0$ Å), the local CO_2 density is over that of vapor CO_2. This corresponds to the suspended surface of liquid droplet within the region of pillared groove.

The contact angles of the CO_2 droplet on the Cu-like surfaces are determined by using a geometrical construction[42, 53]. In this method, a circular function is utilized to fit the density contour of the CO_2 droplet. Here, an iso-density line of 0.01 molecules/Å^3 is adopted to identify the surface of liquid CO_2 droplet. A tangential line near the contact edge is drawn from the circular fit of droplet surface for determining the contact angle. Figure 6 presents the calculated contact angle of liquid CO_2 droplet as a function of ε_{Cu-CO_2} for both flat and pillar-structured surfaces with $w = 10.7$ Å. As is expected, the contact angle of CO_2 droplet is strongly dependent on ε_{Cu-CO_2}. When CO_2 droplet is placed on smooth Cu-like surfaces, the contact angle linearly reduces from around 140° - 62° as ε_{Cu-CO_2} is increased from 0.005 - 0.011 eV, covering the critical point of transition from CO_2-phobic to CO_2-philic. A critical value of $\varepsilon_{Cu-CO_2} = 0.009$ eV is considered as the boundary between CO_2-phobic to CO_2-philic behavior. Intriguingly, as CO_2 droplet is placed on pillar-structured Cu-like surfaces, the contact angle of CO_2 droplet monotonically declines from approximately 180° - 100° with increasing ε_{Cu-CO_2} from 0.005 - 0.011 eV, differing from the case of smooth Cu-like surface. It is clearly observed that the contact angle of CO_2 droplet is greatly enhanced as the solid Cu-like surface becomes pillar-structured rough. For instance, when $\varepsilon_{Cu-CO_2} = 0.005$ eV, the contact angle of CO_2 droplet is able to increase from 140° - 180° with the contact surface changing from smooth to pillar-structured. Such pillar-structured surface shows full CO_2-phobicity. Moreover, when $\varepsilon_{Cu-CO_2} = 0.010$ eV, by pillar-structuring of the Cu-like surface, a shift of transition from CO_2-philicity to CO_2-phobicity can be also achieved. This clearly demonstrates that the wettability of Cu-like surface by

liquid CO_2 can be finely tuned by pillar-structuring engineering. Such tunability in wettability by surface roughening has previously been observed for both natural and artificial liquid water/solid surface systems[21-22, 24-25, 43].

Both experimental and theoretical investigations revealed that the topography of the solid substrates shows influence on the wetting state and the contact angle of water droplets[24-25, 43-46]. To examine whether there is a variation of wetting behavior of liquid CO_2 droplet with the change of surface topography, pillar-structured Cu-like surfaces with varying inter-pillar spacing w and pillar width w from 10.7 - 71.4 Å are constructed. It is noted that all pillar-structured surfaces maintain identical top surface area. Figure 7a-d shows the side-viewed snapshots of CO_2 droplets on pillar-structured Cu-like surfaces with $\varepsilon_{Cu-CO_2} = 0.008$ eV, 0.009 eV, 0.010 eV and 0.011 eV at $t = 50$ ns from MD simulations, respectively. It is observed wetting-mode multiplicity that is pronouncedly sensitive to the topography of the Cu-like surface and ε_{Cu-CO_2}. When $\varepsilon_{Cu-CO_2} = 0.008$ eV (0.009 eV), a critical transition from the Cassie to the Wenzel state occurs, depending on the inter-pillar distance w and pillar width w. As $w < 71.4$ Å (42.9 Å), the liquid CO_2 droplet favors the Cassie state, while it adopts the Wenzel state as $w \geq 71.4$Å (42.9 Å). For the Cassie state, when w is small, the liquid CO_2 droplet does not permeate into the inter-pillared groove. This is due to the fact that the small gaps restrict the liquid CO_2 cluster to move down inter-pillared groove. Once w is enlarged to critical value, for example, $w = 42.9$ Å, partial liquid CO_2 droplet permeates into the inter-pillared groove, although the liquid CO_2 droplet is in the Cassie state. This partial permeation results in negligible change in the contact angle of the liquid CO_2 droplet. When w is large enough, the liquid CO_2 droplet becomes the Wenzel state. With regard to $\varepsilon_{Cu-CO_2} = 0.010$ eV, the liquid CO_2 droplet does not favor the Cassie state. Instead, all pillared surfaces with different topographies show the Wenzel state of the supported liquid CO_2 droplet. However, the Wenzel state CO_2 droplets display different morphologies. Similarly, as $\varepsilon_{Cu-CO_2} = 0.011$ eV, the liquid CO_2 droplets are in the Wenzel state but show different morphology for

all pillared surfaces. Intriguingly, for the two smallest w, the liquid CO_2 droplets completely permeate into the pillared-groove, showing fully wetting behavior. With regard to large w, however, the pillar-structured surfaces are partially wet by the liquid CO_2 droplet. To examine if the transition is caused by the ratio between pillar distance and droplet size, a bigger MD simulation with a bigger droplet at $w = 5.36$ nm and $\varepsilon_{Cu-CO_2} = 0.011$ eV is performed (see bottom of Figure 7d and Supporting information video 1). This additional simulation reveals that this effect remains at larger droplet size, i.e. it is an effect due to ratio between droplet size and pillar size. This implies that macroscopic CO_2 droplet tends to remain Wenzel state on a specific nanopillared surface, which is promising for the practical CO_2 capture by CO_2 condensation on nanostructured surfaces.

Figure 8a-d shows the development of interaction energy between CO_2 and Cu-like substances E_{Cu-CO_2} with $\varepsilon_{Cu-CO_2} = 0.008$ eV, 0.009 eV, 0.010 eV and 0.011 eV during the MD simulation of 50 ns, respectively. Apparently, the evolution of E_{Cu-CO_2} is strongly dependent on the topography of the Cu-like surface, indicating their distinct wetting processes. Based on the curves, two wetting stages can be roughly identified. The first wetting stage is characterized by the remarkable variations of E_{Cu-CO_2} in the curves. In this stage, E_{Cu-CO_2} declines stepwise with MD relaxation time, explaining that the wetting of Cu-like surface is non-uniformly proceeded. A sudden drop of E_{Cu-CO_2} corresponds to a rapid wetting process of pillared surfaces by the liquid CO_2 droplet. This rapid wetting results in notable change in COMP and morphology of the liquid CO_2 droplet. The second stage is characterized by slight oscillations of E_{Cu-CO_2} at constant values. This indicates relative stability of the dynamic wetting behaviors. Accordingly, it is revealed that the MD relaxation time requiring to reach to a stable wetting state is greatly dependent on the coupled topography of Cu-like surface and E_{Cu-CO_2}. For example, the CO_2 liquid droplet wetting of pillar-structured surface with $\varepsilon_{Cu-CO_2} = 0.011$ eV and $w = 71.4$ Å requires maximum MD relaxation time of 35 ns. By comparison, it is observed that different

simulated systems result in differences in the E_{Cu-CO_2} of the second stage. For pillar-structured surfaces with a given w, the big different magnitudes of E_{Cu-CO_2} primarily come from different ε_{Cu-CO_2}. As for pillar-structured surfaces with a given ε_{Cu-CO_2}, the significant differences of E_{Cu-CO_2} explain their different wetting morphologies of the liquid CO_2 droplet. For example, when $\varepsilon_{Cu-CO_2} = 0.008$ eV, E_{Cu-CO_2} increases with w varying from 10.7 - 53.6 Å due to different solid-liquid contact areas, whereas for $w = 71.4$ Å, E_{Cu-CO_2} inversely drops to minimum value of -175 eV because the Wenzel state of the liquid CO_2 droplet significantly increases the solid-liquid contact area.

4. Conclusions

Large-scale classic MD simulations are performed to reveal the role of nanoscale surface and topographical features on the wetting characteristic of CO_2 droplet on Cu-like surfaces. For reference, the wetting morphology of liquid CO_2 droplet on smooth Cu-like surface is initially investigated. As a result of vaporization, the distribution between vapor and liquid CO_2 is governed by the phase equilibrium. The wetting morphology of liquid CO_2 droplet is strongly sensitive to ε_{Cu-CO_2}. Specifically, a linear relationship between the intrinsic contact angle of liquid CO_2 droplet and ε_{Cu-CO_2} is revealed. For a given ε_{Cu-CO_2}, however, Cu-like surfaces with periodically pillared structures significantly rise the contact angle of liquid CO_2 droplet, resulting from that less liquid-solid contact area leads to weaker interactions between liquid CO_2 droplet and the solid substrate. Notably, by pillared nanostructuring of surface, it is observed a critical transition of CO_2-philic to CO_2-phobic. Interestingly, by either changing ε_{Cu-CO_2} or structural parameter of pillared surfaces, a crossover of wetting state from the Cassie state to the Wenzel state appears. It can be inferred that the wetting state on a solid substrate can be tuned by surface roughening. The results of this work provide important insights into the contact angle and wetting behaviors of liquid CO_2 droplet on solid surfaces that is

difficult to obtain by experimental characterizations, which will enlighten future attempts to design CO_2-phobic surfaces for important CO_2 capture applications.

Acknowledgments

References

1.   Aresta, M.; Dibenedetto, A.; Angelini, A., Catalysis for the Valorization of Exhaust Carbon: From CO_2 to Chemicals, Materials, and Fuels. Technological Use of CO_2. *Chemical Reviews* **2014**, *114*, 1709-1742.

2.   Darensbourg, D. J., Making Plastics from Carbon Dioxide: Salen Metal Complexes as Catalysts for the Production of Polycarbonates from Epoxides and CO_2. *Chemical Reviews* **2007**, *107*, 2388-2410.

3.   Olah, G. A.; Goeppert, A.; Prakash, G. K. S., Chemical Recycling of Carbon Dioxide to Methanol and Dimethyl Ether: From Greenhouse Gas to Renewable, Environmentally Carbon Neutral Fuels and Synthetic Hydrocarbons. *The Journal of Organic Chemistry* **2009**, *74*, 487-498.

4.   Leung, D. Y. C.; Caramanna, G.; Maroto-Valer, M. M., An Overview of Current Status of Carbon Dioxide Capture and Storage Technologies. *Renewable and Sustainable Energy Reviews* **2014**, *39*, 426-443.

5.   Rubin, E. S.; Davison, J. E.; Herzog, H. J., The Cost of CO2 Capture and Storage. *International Journal of Greenhouse Gas Control* **2015**, *40*, 378-400.

6.   Song, C.; Liu, Q.; Ji, N.; Deng, S.; Zhao, J.; Li, Y.; Song, Y.; Li, H., Alternative Pathways for Efficient CO_2 Capture by Hybrid Processes—a Review. *Renewable and Sustainable Energy Reviews* **2018**, *82*, 215-231.

7.   Olajire, A. A., CO2 Capture and Separation Technologies for End-of-Pipe Applications – a Review. *Energy* **2010**, *35*, 2610-2628.

8.   Bishnoi, S.; Rochelle, G. T., Absorption of Carbon Dioxide in Aqueous Piperazine/Methyldiethanolamine. *AIChE Journal* **2002**, *48*, 2788-2799.

9.   Sreedhar, I.; Nahar, T.; Venugopal, A.; Srinivas, B., Carbon Capture by Absorption – Path Covered and Ahead. *Renewable and Sustainable Energy Reviews* **2017**, *76*, 1080-1107.

10.   Zhao, L.; Primabudi, E.; Stolten, D., Investigation of a Hybrid System for Post-Combustion Capture. *Energy Procedia* **2014**, *63*, 1756-1772.

11.   Ben-Mansour, R.; Habib, M. A.; Bamidele, O. E.; Basha, M.; Qasem, N. A. A.; Peedikakkal, A.; Laoui, T.; Ali, M., Carbon Capture by Physical Adsorption: Materials, Experimental Investigations and Numerical Modeling and Simulations – a Review. *Applied Energy* **2016**, *161*, 225-255.

12.   Gao, W.; Zhou, T.; Gao, Y.; Louis, B.; O'Hare, D.; Wang, Q., Molten Salts-Modified Mgo-Based Adsorbents for Intermediate-Temperature CO_2 Capture: A Review. *Journal of Energy Chemistry* **2017**, *26*, 830-838.

13.   Samanta, A.; Zhao, A.; Shimizu, G. K. H.; Sarkar, P.; Gupta, R., Post-Combustion CO_2 Capture Using Solid Sorbents: A Review. *Industrial & Engineering Chemistry Research* **2012**, *51*, 1438-1463.

14.   Hussain, A.; Hägg, M.-B., A Feasibility Study of CO_2 Capture from Flue Gas by a Facilitated Transport Membrane. *Journal of Membrane Science* **2010**, *359*, 140-148.

15.   Merkel, T. C.; Lin, H.; Wei, X.; Baker, R., Power Plant Post-Combustion Carbon Dioxide Capture: An Opportunity for Membranes. *Journal of Membrane Science* **2010**, *359*, 126-139.

16.   Scholes, C. A.; Kentish, S. E.; Stevens, G. W., The Effect of Condensable Minor Components on the Gas Separation Performance of Polymeric Membranes for Carbon Dioxide Capture. *Energy Procedia* **2009**, *1*, 311-317.

17.   Sreedhar, I.; Vaidhiswaran, R.; Kamani, B. M.; Venugopal, A., Process and Engineering Trends in Membrane Based Carbon Capture. *Renewable and Sustainable Energy Reviews* **2017**, *68*, 659-684.

18.   Ma, Z. W.; Zhang, P.; Bao, H. S.; Deng, S., Review of Fundamental Properties of CO_2 Hydrates and CO_2 Capture and Separation Using Hydration Method. *Renewable and Sustainable Energy Reviews* **2016**, *53*, 1273-1302.

19.   Park, S.; Lee, S.; Lee, Y.; Seo, Y., CO_2 Capture from Simulated Fuel Gas Mixtures Using Semiclathrate Hydrates Formed by Quaternary Ammonium Salts. *Environmental Science & Technology* **2013**, *47*, 7571-7577.

20.   Sun, Q.; Kang, Y. T., Review on CO_2 Hydrate Formation/Dissociation and Its Cold Energy Application. *Renewable and Sustainable Energy Reviews* **2016**, *62*, 478-494.

21.   Zhang, S.; Huang, J.; Chen, Z.; Lai, Y., Bioinspired Special Wettability Surfaces: From Fundamental Research to Water Harvesting Applications. *Small* **2017**, *13*, 1602992.

22.   Jin, Y.; Zhang, L.; Wang, P., Atmospheric Water Harvesting: Role of Surface Wettability and Edge Effect. *Global Challenges* **2017**, *1*, 1700019.

23.   Lee, A.; Moon, M.-W.; Lim, H.; Kim, W.-D.; Kim, H.-Y., Water Harvest Via Dewing. *Langmuir* **2012**, *28*, 10183-10191.

24.   Gao, S.; Liu, W.; Liu, Z., Tuning Nanostructured Surfaces with Hybrid Wettability Areas to Enhance Condensation. *Nanoscale* **2019**, *11*, 459-466.

25.   Snustad, I.; Røe, I. T.; Brunsvold, A.; Ervik, Å.; He, J.; Zhang, Z., A Review on Wetting and Water Condensation - Perspectives for CO_2 condensation. *Advances in Colloid and Interface Science* **2018**, *256*, 291-304.

26.   Wu, J.; Ervik, Å.; Snustad, I.; Xiao, S.; Brunsvold, A.; He, J.; Zhang, Z., Contact Angle and Condensation of a CO_2 Droplet on a Solid Surface. *The Journal of Physical Chemistry C* **2019**, *123*, 443-451.

27.   van Bergen, F.; Gale, J.; Damen, K. J.; Wildenborg, A. F. B., Worldwide Selection of Early Opportunities for CO_2-Enhanced Oil Recovery and CO_2-Enhanced Coal Bed Methane Production. *Energy* **2004**, *29*, 1611-1621.

28.   Kuuskraa, V. A.; Godec, M. L.; Dipietro, P., CO_2 Utilization from "Next Generation" CO_2 Enhanced Oil Recovery Technology. *Energy Procedia* **2013**, *37*, 6854-6866.

29.   Alvarado, V.; Manrique, E., Enhanced Oil Recovery: An Update Review. *Energies* **2010**, *3*, 1529-1575.

30.   Wu, J.; He, J.; Torsater, O.; Zhang, Z., Effect of Nanoparticles on Oil-Water Flow in a Confined Nanochannel: A Molecular Dynamics Study. In *SPE International Oilfield Nanotechnology Conference and Exhibition*, Society of Petroleum Engineers: Noordwijk, The Netherlands, 2012; p 16.

31.   Liu, S.; Yang, X.; Qin, Y., Molecular Dynamics Simulation of Wetting Behavior at CO_2/Water/Solid Interfaces. *Chinese Science Bulletin* **2010**, *55*, 2252-2257.

32.   Kaveh, N. S.; Rudolph, E. S. J.; van Hemert, P.; Rossen, W. R.; Wolf, K. H., Wettability Evaluation of a CO_2/Water/Bentheimer Sandstone System: Contact Angle, Dissolution, and Bubble Size. *Energy & Fuels* **2014**, *28*, 4002-4020.

33.   Tenney, C. M.; Cygan, R. T., Molecular Simulation of Carbon Dioxide, Brine, and Clay Mineral Interactions and Determination of Contact Angles. *Environmental Science & Technology* **2014**, *48*, 2035-2042.

34.   Chen, C.; Wan, J.; Li, W.; Song, Y., Water Contact Angles on Quartz Surfaces under Supercritical CO_2 Sequestration Conditions: Experimental and Molecular Dynamics Simulation Studies. *International Journal of Greenhouse Gas Control* **2015**, *42*, 655-665.

35.   Chen, C.; Zhang, N.; Li, W.; Song, Y., Water Contact Angle Dependence with Hydroxyl Functional Groups on Silica Surfaces under CO_2 Sequestration Conditions. *Environmental Science & Technology* **2015**, *49*, 14680-14687.

36.   Javanbakht, G.; Sedghi, M.; Welch, W.; Goual, L., Molecular Dynamics Simulations of CO_2/Water/Quartz Interfacial Properties: Impact of CO_2 Dissolution in Water. *Langmuir* **2015**, *31*, 5812-5819.

37.   Chen, C.; Dong, B.; Zhang, N.; Li, W.; Song, Y., Pressure and Temperature Dependence of Contact Angles for CO_2/Water/Silica Systems Predicted by Molecular Dynamics Simulations. *Energy & Fuels* **2016**, *30*, 5027-5034.

38.   Liu, B.; Shi, J.; Wang, M.; Zhang, J.; Sun, B.; Shen, Y.; Sun, X., Reduction in Interfacial Tension of Water–Oil Interface by Supercritical CO_2 in Enhanced Oil Recovery Processes Studied with Molecular Dynamics Simulation. *The Journal of Supercritical Fluids* **2016**, *111*, 171-178.

39.   Yan, Y.; Li, C.; Dong, Z.; Fang, T.; Sun, B.; Zhang, J., Enhanced Oil Recovery Mechanism of CO_2 Water-Alternating-Gas Injection in Silica Nanochannel. *Fuel* **2017**, *190*, 253-259.

40.   Abramov, A.; Keshavarz, A.; Iglauer, S., Wettability of Fully Hydroxylated and Alkylated (001) A-Quartz Surface in Carbon Dioxide Atmosphere. *The Journal of Physical Chemistry C* **2019**, *123*, 9027-9040.

41.   Yan, M.; Yang, X.; Lu, Y., Wetting Behavior of Water Droplet on Solid Surfaces in Solvent Environment: A Molecular Simulation Study. *Colloids and Surfaces A: Physicochemical and Engineering Aspects* **2013**, *429*, 142-148.

42.   Iglauer, S.; Mathew, M. S.; Bresme, F., Molecular Dynamics Computations of Brine–CO_2 Interfacial Tensions and Brine–CO_2–Quartz Contact Angles and Their Effects on Structural and Residual Trapping Mechanisms in Carbon Geo-Sequestration. *Journal of Colloid and Interface Science* **2012**, *386*, 405-414.

43.   Yan, Y. Y.; Gao, N.; Barthlott, W., Mimicking Natural Superhydrophobic Surfaces and Grasping the Wetting Process: A Review on Recent Progress in Preparing Superhydrophobic Surfaces. *Advances in Colloid and Interface Science* **2011**, *169*, 80-105.

44.   Bhushan, B.; Koch, K.; Jung, Y. C., Nanostructures for Superhydrophobicity and Low Adhesion. *Soft Matter* **2008**, *4*, 1799-1804.

45.   Koishi, T.; Yasuoka, K.; Fujikawa, S.; Ebisuzaki, T.; Zeng, X. C., Coexistence and Transition between Cassie and Wenzel State on Pillared Hydrophobic Surface. *Proceedings of the National Academy of Sciences* **2009**, *106*, 8435-8440.

46.   Lundgren, M.; Allan, N. L.; Cosgrove, T.; George, N., Molecular Dynamics Study of Wetting of a Pillar Surface. *Langmuir* **2003**, *19*, 7127-7129.

47.   Mishin, Y.; Mehl, M. J.; Papaconstantopoulos, D. A.; Voter, A. F.; Kress, J. D., Structural Stability and Lattice Defects in Copper: Ab Initio, Tight-Binding, and Embedded-Atom Calculations. *Physical Review B* **2001**, *63*, 224106.

48.   Daw, M. S.; Baskes, M. I., Embedded-Atom Method: Derivation and Application to Impurities, Surfaces, and Other Defects in Metals. *Physical Review B* **1984**, *29*, 6443-6453.

49.   Avendaño, C.; Lafitte, T.; Galindo, A.; Adjiman, C. S.; Jackson, G.; Müller, E. A., Saft-Γ Force Field for the Simulation of Molecular Fluids. 1. A Single-Site Coarse Grained Model of Carbon Dioxide. *The Journal of Physical Chemistry B* **2011**, *115*, 11154-11169.

50.   Hoang, H.; Delage-Santacreu, S.; Galliero, G., Simultaneous Description of Equilibrium, Interfacial, and Transport Properties of Fluids Using a Mie Chain Coarse-Grained Force Field. *Industrial & Engineering Chemistry Research* **2017**, *56*, 9213-9226.

51.   Müller, E. A.; Jackson, G., Force-Field Parameters from the Saft-Γ Equation of State for Use in Coarse-Grained Molecular Simulations. *Annual Review of Chemical and Biomolecular Engineering* **2014**, *5*, 405-427.

52.   Yuan, Y.; Lee, T. R., Contact Angle and Wetting Properties. In *Surface Science Techniques*, Bracco, G.; Holst, B., Eds. Springer Berlin Heidelberg: Berlin, Heidelberg, 2013; pp 3-34.

53.   Bresme, F.; Quirke, N., Computer Simulation Study of the Wetting Behavior and Line Tensions of Nanometer Size Particulates at a Liquid-Vapor Interface. *Physical Review Letters* **1998**, *80*, 3791-3794.

Figures and captions
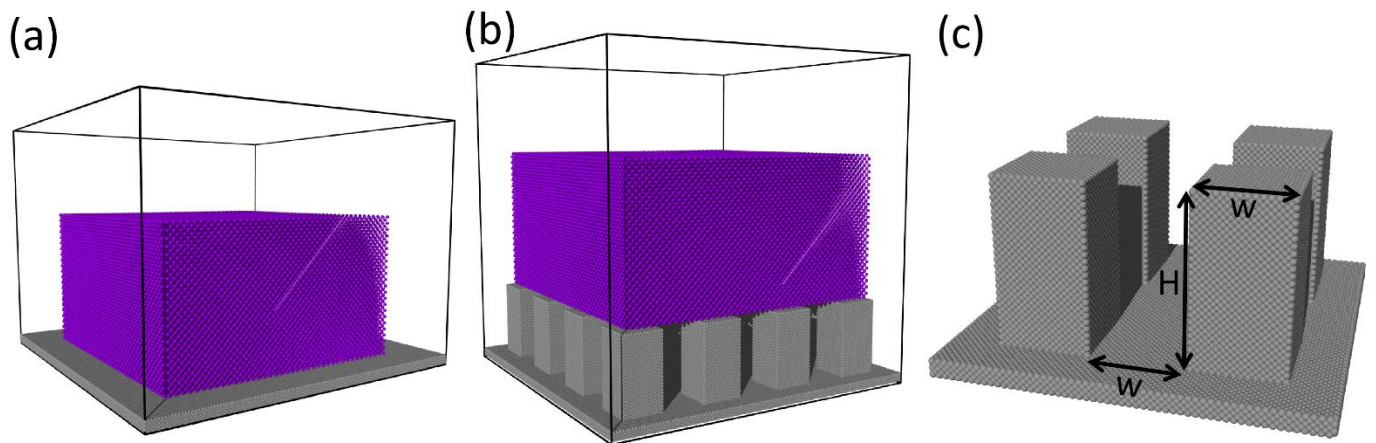
Figure 1 Initial configurations of CO_2 wetting simulations on (a) a flat Cu-like surface (b) a pillar-structured Cu-like surface. (c) Atomic models of a pillar-structured Cu-like surface.
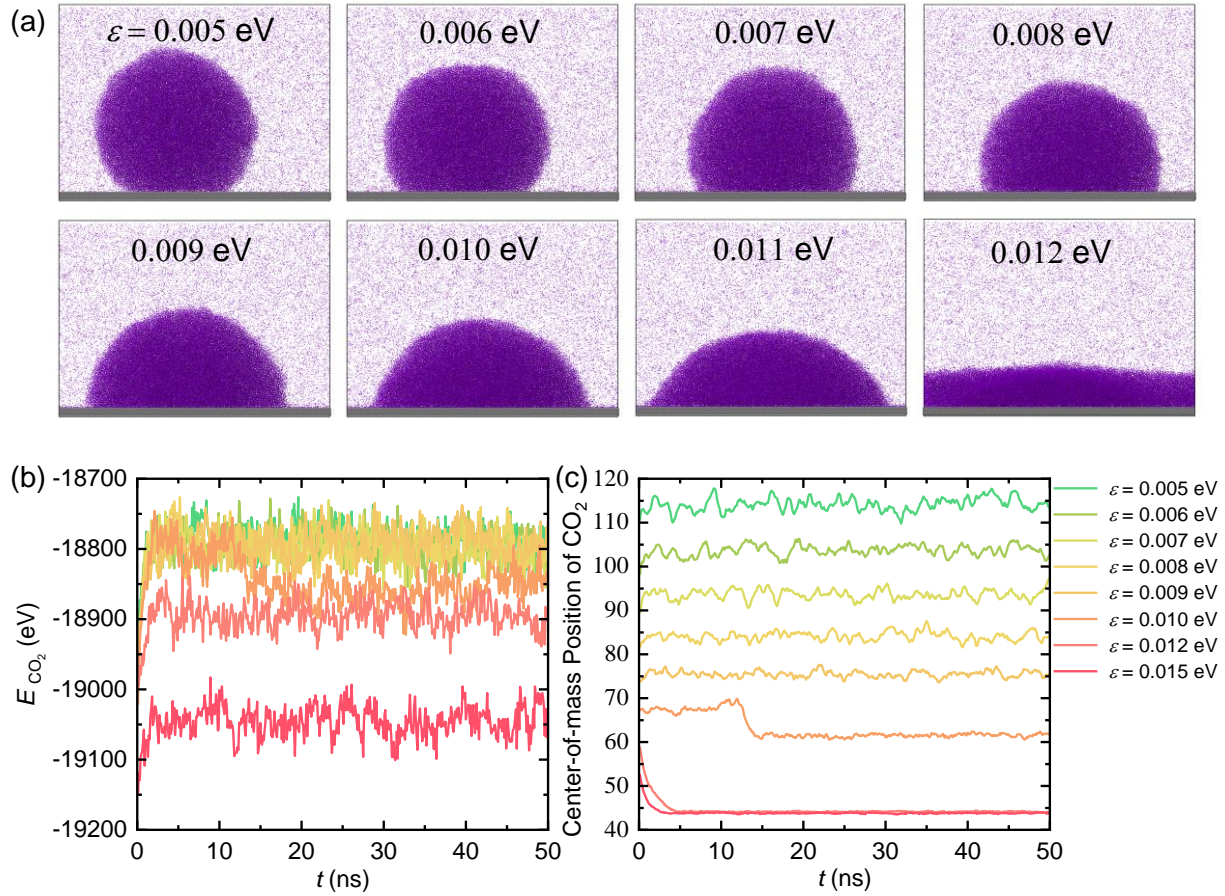
Figure 2 CO_2 wetting on Cu-like substrates. (a) Wetting morphologies of a CO_2 droplet on smooth Cu-like surface with interaction energy parameter ε_{Cu-CO_2} between CO_2 and Cu-like surface varying from 0.005 - 0.012 eV. (b) The total potential energies E_{CO_2} develops with MD simulation times in the CO_2/Cu-like surface systems. (c) Change in the z-directional center-of-mass positions (COMPs) of CO_2 with MD simulation times for CO_2/Cu-like surface systems.
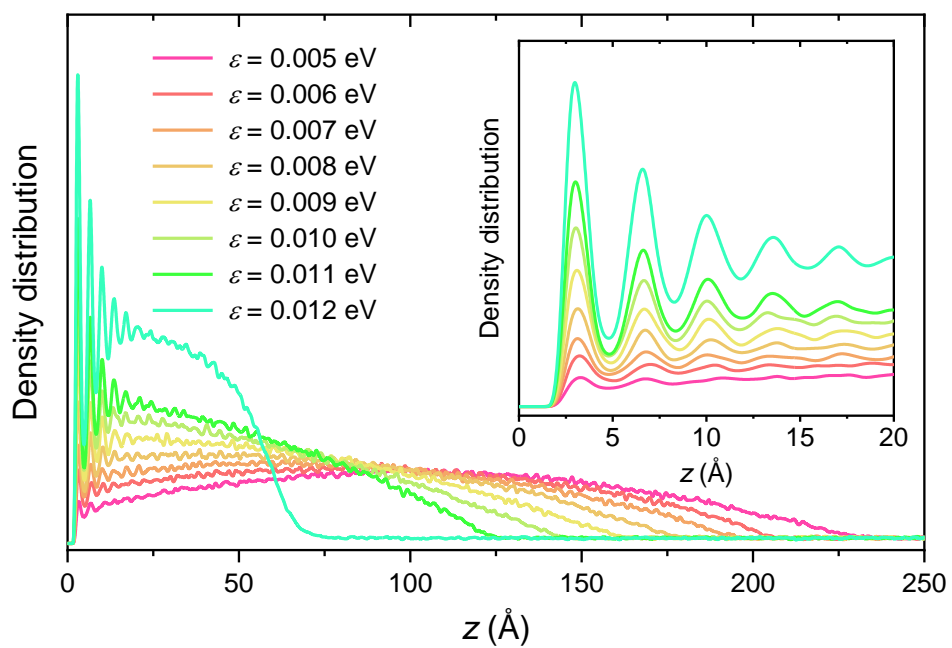
Figure 3 Relative density profiles of CO_2 from the Cu-like surface to the top CO_2 vapor phase. Inset is the zoomed-in plots of relative density profiles near the Cu-like surfaces.
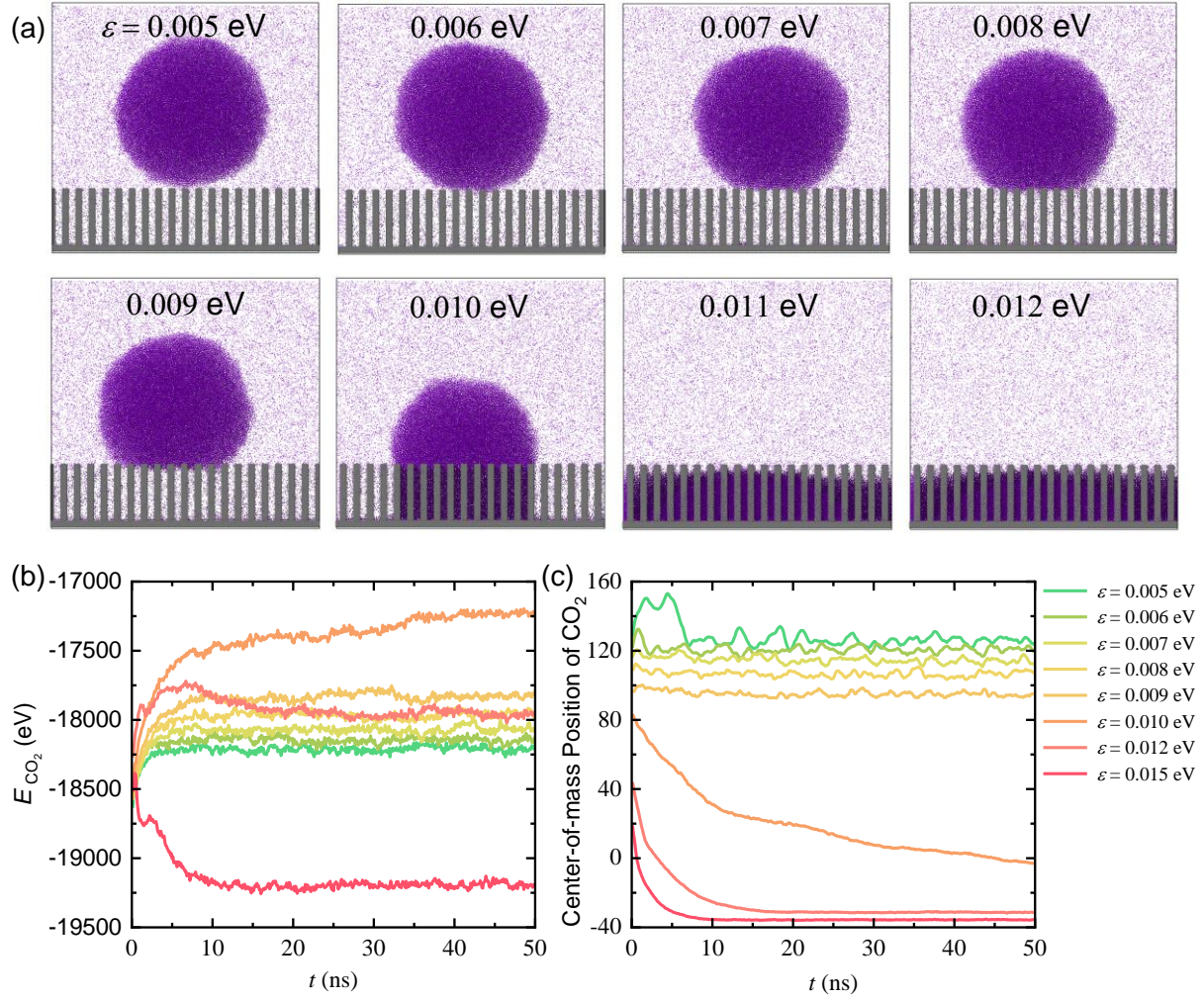
Figure 4 Wetting characteristics of a CO_2 droplet on a nanopillar-structured surface with structural parameter $w = 10.7$ Å. (a) Wetting morphologies of a CO_2 droplet with varying interaction energy parameter ε_{Cu-CO_2} from 0.005 - 0.012 eV. (b) The development of total potential energies E_{CO_2} during the whole MD simulation for the CO_2/Cu-like surface systems. (c) Variation of the z-directional center-of-mass positions (COMPs) of CO_2 during the MD wetting simulation for CO_2/Cu-like surface systems.
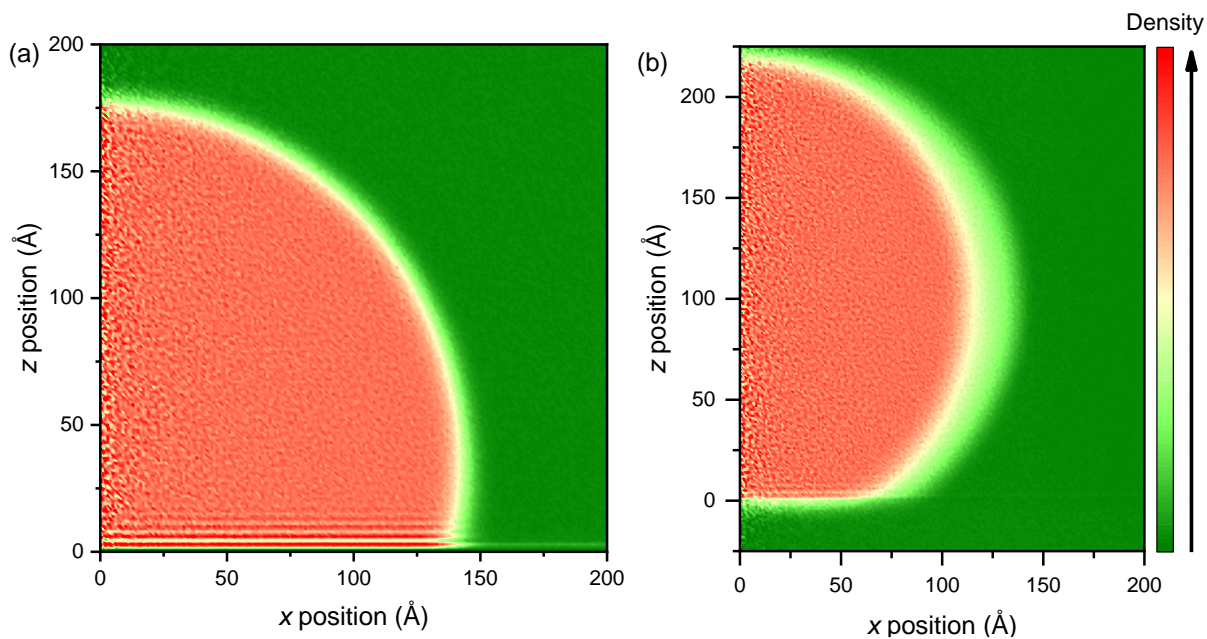
Figure 5 Two representative relative density contours of CO_2 droplet on (a) a smooth Cu-like surface and (b) a pillar-structured surface with structural parameter $w = 10.7$ Å. Both systems have identical interaction energy parameter $\varepsilon_{Cu-CO_2} = 0.008$ eV.
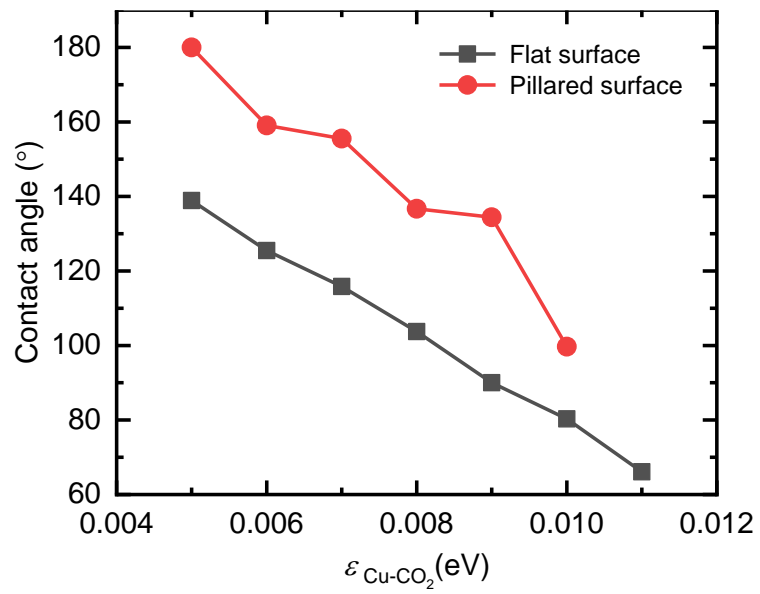
Figure 6 Contact angles of CO_2 droplet as a function of interaction energy parameter ε_{Cu-CO_2} for both CO_2/flat substrate and CO_2/pillar-structured substrate systems.
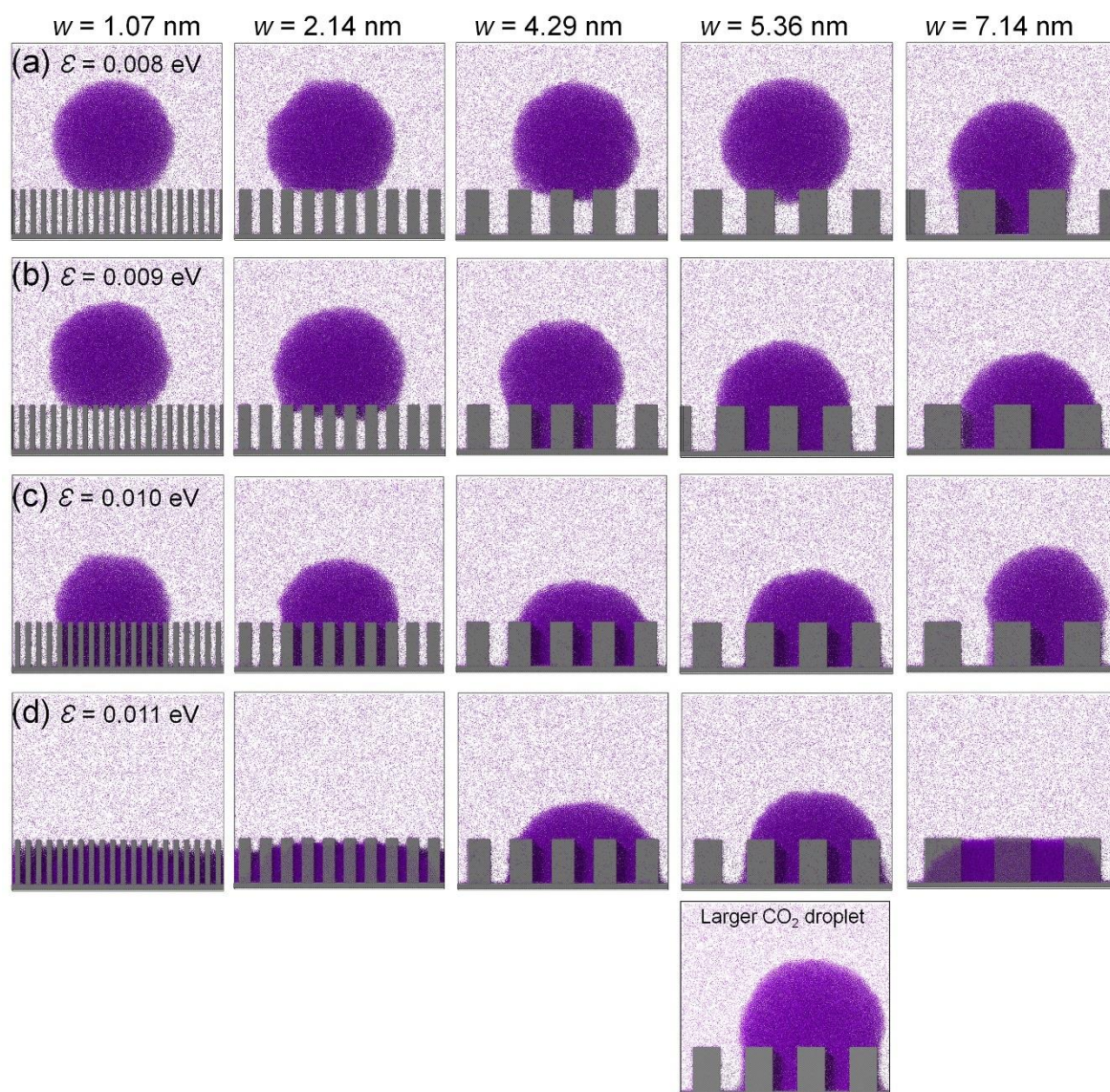
Figure 7 Comparison of wetting morphology of CO_2 droplet on different roughened surfaces. The roughened surfaces are pillar-structured Cu-like surfaces with structural parameter $w = 1.07, 2.14, 4.29, 5.36$ and 7.14 nm, and interaction energy parameter ε_{Cu-CO_2} (a) $= 0.008$ eV, (b) $= 0.009$ eV, (c) $= 0.010$ eV and (d) $= 0.011$ eV, respectively. Bottom: A big MD simulation shows that the transition of wetting is caused by the ratio between droplet size and pillar size.
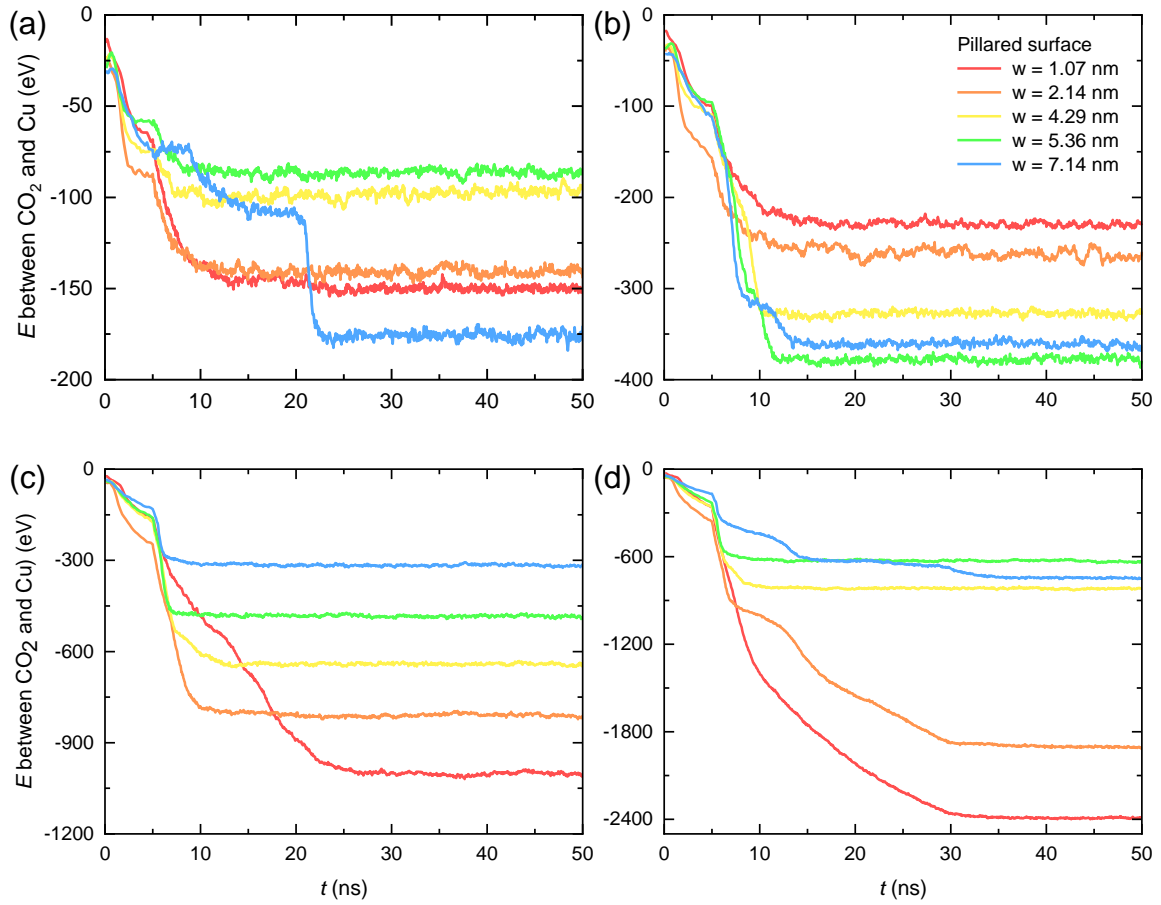
Figure 8 The evolution of interaction energies E_{Cu-CO_2} between CO_2 and pillar-structured Cu-like surfaces during the MD wetting simulations, where the interaction energy parameter ε_{Cu-CO_2} are taken as (a) 0.008 eV, (b) 0.009 eV, (c) 0.010 eV and (d) 0.011 eV, respectively.